Pulsed Field Magnetization of Large MgB_2 Bulk Fabricated by Reactive Liquid Mg Infiltration

2012 Jpn. J. Appl. Phys. 51 103005

(http://iopscience.iop.org/1347-4065/51/10R/103005)

Japanese Journal of Applied Physics **51** (2012) 103005 **REGULAR PAPER**
http://dx.doi.org/**10.1143/JJAP.51.103005**

Pulsed Field Magnetization of Large MgB_2 Bulk Fabricated by Reactive Liquid Mg Infiltration

Hiroyuki Fujishiro[1]*, Takuya Tamura[1], Takahiro Arayashiki[1], Mitsuru Oyama[1], Tomohisa Sasaki[1], Tomoyuki Naito[1], Giovanni Giunchi[2], and Alessandro Figini Albisetti[2]

[1] *Faculty of Engineering, Iwate University, Morioka 020-8551, Japan*
[2] *EDISON S.p.A., R&D Division, Foro Buonaparte 31, 20121 Milano, Italy*

Received June 3, 2012; accepted August 10, 2012; published online October 3, 2012

Pulsed field magnetization (PFM) was performed for the first time on a large MgB_2 bulk 50 mm diameter fabricated by a reactive liquid Mg infiltration (Mg-RLI) method, and the time dependence of the local field $B_L^C(t)$ and the trapped field profiles were measured. The trapped field of $B_z = 0.47$ T and the total trapped flux of $\Phi = 0.50$ mWb were achieved at $T_s = 23$ K and both values decreased with increasing temperature T_s. The experimental results can be qualitatively reproduced by numerical simulation using electromagnetic and thermal fields for PFM. The flux dynamics and the heat generation/propagation in the MgB_2 bulk during PFM were in clear contrast with those in REBaCuO superconducting bulks because of the large thermal conductivity, small specific heat, and narrow temperature margin against the transition temperature T_c.

1. Introduction

The superconducting bulk magnet using an REBaCuO (RE: rare earth element or Y) bulk can be used for practical applications such as sputtering cathodes,[1)] magnetic separation,[2)] and drug delivery systems.[3)] The REBaCuO bulks with 45–60 mm diameters are commercially available to produce tesla-order quasi-permanent magnets, which are fabricated by a melt textured method. Although a large single-domain bulk of over 100 mm in diameter is difficult to fabricate, large bulks have recently been realized only by a multiseeding technique.[4)]

MgB_2 bulk also has a promising potential as a quasi-permanent magnet because the problem of weak links at the grain boundaries can be ignored even in the polycrystalline samples owing to their long coherence length, ξ.[5)] The MgB_2 bulk enables us to realize better and larger polycrystalline bulk magnets below the transition temperature T_c. Several groups have already reported a trapped field on the MgB_2 bulk by field-cooled magnetization (FCM). A trapped field value of $B_z = 2.3$ T was obtained at 6 K on the MgB_2 bulk of 28 mm diameter and 11 mm thickness, which was sintered under a high pressure of 2 GPa.[6)] Yamamoto *et al.* reported a 1.2 T MgB_2 magnet (20 mm in diameter and 5 mm in thickness) magnetized by FCM at 17 K, and a 3 T-class magnet, which consisted of doubly stacked MgB_2 bulks.[7)] One of the authors (G. Giunchi) has developed MgB_2 bulks by the reactive Mg liquid infiltration (Mg-RLI) technique,[8)] which is preferable to fabricate dense and large MgB_2 bulk disks and cylinders, where the maximum B_z value was about 1.3 T at 15 K by FCM on the Mg-RLI-MgB_2 bulk of 55 mm diameter and 15 mm thickness at the center hole of 6 mm.[9)]

Pulsed field magnetization (PFM) is an another technique to magnetize bulk superconductors. However, for the REBaCuO bulks, the trapped field B_z achievable by PFM is nonetheless lower than that achievable by FCM because of the large temperature rise caused by the dynamical motion of the magnetic flux. Several approaches have been performed and succeeded in enhancing B_z using multipulse techniques.[10,11)] We have experimentally examined the time and spatial dependences of the temperature $T(t,x)$, the local field $B_z(t,x)$, and the trapped field B_z on the surface of cryocooled REBaCuO bulks during PFM for various starting temperatures T_s and applied fields B_{ex}.[12–14)] To enhance B_z, the reduction in temperature rise and the lowering of T_s are effective because of the enhancement of the critical current density J_c, similarly to the case for FCM. Considering the obtained experimental results, we proposed a new PFM technique named the modified multipulse technique with stepwise cooling (MMPSC)[15)] and successfully realized the highest field trap of $B_z = 5.20$ T on a GdBaCuO bulk of 45 mm diameter at 30 K,[16)] which is a record-high value achieved by PFM to date. Recently, we have demonstrated the numerical simulation of PFM for a cryocooled REBaCuO bulk disk, where the results of the simulation reproduced the experimental ones qualitatively.[17–19)] However, the PFM procedure for the MgB_2 bulk has not yet been reported.

In this study, we applied the PFM technique to a large MgB_2 bulk of 50 mm diameter for various applied fields B_{ex} and temperatures T_s. The PFM procedure for the MgB_2 bulk is a first and systematic approach to enhance B_z. The numerical simulation for PFM was also performed for the MgB_2 bulk. Since the operation temperature of the MgB_2 bulk is fairly lower than that of REBaCuO, the thermal properties of the MgB_2 bulk such as the specific heat and the thermal conductivity are quite different. As a result, the PFM performance is expected to be quite different. We discuss the characteristics of PFM on the MgB_2 bulk, compared with those on the REBaCuO bulk.

2. Experimental Procedure

The MgB_2 bulk disk used in this study was 50 mm in diameter and 16 mm in thickness, which was fabricated by the Mg-RLI technique. The detailed fabrication process was described elsewhere.[8,9)] T_c of the bulk was estimated to be 39 K using a small piece cut from a similar bulk fabricated by the Mg-RLI method.[20)] The bulk was tightly mounted in a stainless steel (SUS316L) ring of 8 mm thickness using a stycast 2850GT resin as a filling. Figure 1 shows the experimental setup around the bulk and the magnetizing pulse coil for PFM. The bulk was set on a soft iron yoke cylinder of 40 mm diameter and 20 mm thickness and tightly anchored onto the cold stage of a Gifford–McMahon (GM) cycle helium refrigerator. The initial temperature T_s of the bulk was set from 18 to 33 K. A magnetizing solenoid coil (94 mm i.d., 153 mm o.d., and 67 mm height), which was dipped in liquid nitrogen, was placed outside the vacuum chamber. A magnetic pulse B_{ex} with a rise time of 0.01 s

*E-mail address: fujishiro@iwate-u.ac.jp

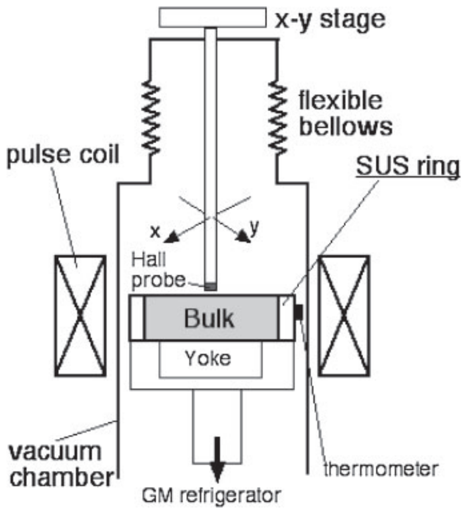

Fig. 1. Experimental setup for PFM around the bulk and the magnetizing coil.

and a duration of 0.1 s was applied to the bulk by flowing the pulsed current from a condenser bank. The time dependence of the applied pulsed field $B_{ex}(t)$ was monitored from the current $I(t)$ flowing in the shunt resister. The time evolutions of the local field $B_L{}^C(t)$ and the subsequent trapped field B_z at the center of the bulk surface were monitored inside the vacuum chamber by an axial-type Hall sensor (F W Bell, BHA 921), which touched the bulk surface, using a digital oscilloscope. Two-dimensional trapped field profiles of B_z (1 mm) were mapped at a distance of $z = 1$ mm above the bulk surface, stepwise with a pitch of 1 mm by scanning the same Hall sensor using an x–y stage controller. During PFM, the time dependence of temperature $T(t)$ was measured at the side surface of the SUS316L ring using a Cernox thermometer.

3. Model of Numerical Simulation for PFM

On the basis of the experimental setup around the MgB_2 bulk for PFM, the framework of the numerical simulation was constructed using the axi-symmetric coordinate. The detailed procedure of the simulation was described elsewhere.[17] The bulk was magnetized using a solenoid-type coil and the sizes of the bulk and the coil were the same as those of the experimental condition. Physical phenomena during PFM were described using electromagnetic and thermal fields, which were taken from ref. 21. The power-n model ($n = 5$) was supposed to describe the nonlinear E–J characteristic in the superconducting bulk. The temperature and magnetic field dependences of the critical current density $J_c(T, B)$ are described as

$$J_c(T, B) = \alpha\left[1 - \left(\frac{T}{T_c}\right)^2\right]^{3/2} \frac{B_0}{|B| + B_0}, \quad (1)$$

where T_c (= 39 K) is the critical temperature at $B = 0$, and B_0 (= 1.3 T) is constant. In eq. (1), the simulation was performed for various α values. As a result, the α value of 5×10^7 was best fitted to reproduce the experimental results, which corresponded to J_c (20 K, 0 T) of 3.2×10^7 Am^{-2}. This J_c value is two orders of magnitude smaller than that of the MgB_2 bulks fabricated by an *in-situ* method.[6,22,23] This difference may come from the deterioration of J_c caused by the inhomogeneous Mg infiltration, as stated in a later section. The time dependence of the applied pulsed field $B_{ex}(t)$ with the rise time of $\tau = 0.01$ s was approximated in the following equation,

$$B_{ex}(t) = B_{ex}\frac{t}{\tau}\exp\left(1 - \frac{t}{\tau}\right). \quad (2)$$

Table I. Numerical values of parameters used in the simulation.

Symbol	Parameter	Value
T_c	Transition temperature in eq. (1)	39 K
$\rho(MgB_2)$	Mass density of MgB_2 bulk	2.59×10^3 kg m^{-3}
ρ(SUS)	Mass density of SUS316L	7.93×10^3 kg m^{-3}
$C(MgB_2)$	Specific heat of MgB_2 bulk at 40 K	1.72×10^1 J kg^{-1} K^{-1}
C(SUS)	Specific heat of SUS316L at 40 K	3.0×10^1 J kg^{-1} K^{-1}
$\kappa(MgB_2)$	Thermal conductivity of MgB_2 bulk at 40 K	80 W m^{-1} K^{-1}
κ(SUS)	Thermal conductivity of SUS316L at 40 K	3 W m^{-1} K^{-1}
n	n-value	5
B_0	Constant in eq. (1)	1.3 T
α	Constant in eq. (1)	5×10^7 A m^{-2}
τ	Rise time of the pulse in eq. (2)	0.01 s
κ_{cont}	Thermal conductivity of spacing plate	0.5 W m^{-1} K^{-1}

The numerical parameters used in the simulation are presented in Table I. The thermal conductivity κ and the specific heat C values of the MgB_2 bulk were presumed to be temperature dependent, as referred from the literature.[20,24] For simplicity, κ and C of the SUS316L ring and the mass densities ρ of MgB_2 and the SUS316L ring were supposed to be constant. We set the spacing plate with a thermal conductivity κ_{cont} of 0.5 W m^{-1} K^{-1} between the bulk and the cold stage (and SUS316L ring), which imaginarily represents both the cooling power of the refrigerator and the thermal contact. Commercial software, Photo-Eddy, combined with Photo-Thermo (Photon Ltd.), was used for analyses of the magnetic field and temperature distribution in the MgB_2 bulk during PFM.

4. Experimental Results

Figure 2 depicts the trapped field B_z at the center of the bulk surface by PFM, as a function of applied pulsed field B_{ex}. At $T_s = 18$ K, the magnetic flux intruded and was trapped at the center of the bulk surface at $B_{ex} \geq 1$ T, the trapped field B_z takes a maximum at $B_{ex} = 1.7$ T and then decreased with increasing B_{ex}. At $T_s \geq 23$ K, B_z showed a similar applied field dependence, and the applied field $B_{ex}{}^0$, at which the magnetic flux starts to be trapped at the bulk center, decreases with increasing T_s. The maximum B_z by PFM was 0.47 T at $T_s = 23$ K in this study. These applied field and temperature dependences of B_z show similar characteristics to those for REBaCuO bulks.[14] However, note that the steep B_{ex} dependence of B_z is a peculiar characteristic of the MgB_2 bulk, compared with that for the REBaCuO bulk, which results from the large thermal conductivity κ, small specific heat C, and narrow temperature margin against the transition temperature T_c in the MgB_2 bulk at T_s. Detailed discussion is performed in §5.

Figure 3 shows the time dependence of the applied field $B_{ex}(t)$ and the local field $B_L{}^C(t)$ at the center of the bulk surface at $T_s = 23$ K for various applied fields B_{ex}. Each condition is indicated in Fig. 2, as the symbols of (a) to (d).

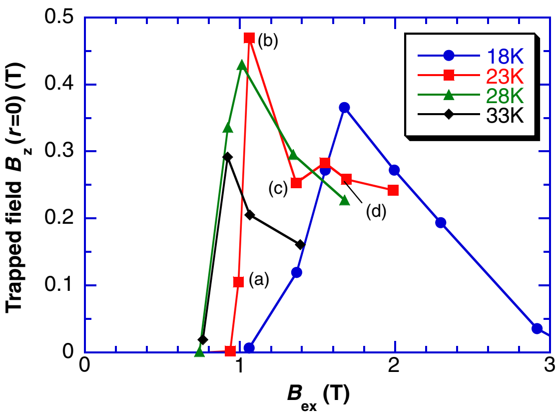

Fig. 2. (Color online) Trapped field B_z at the center of the MgB_2 bulk surface by PFM for each starting temperature T_s, as a function of applied pulsed field B_{ex}.

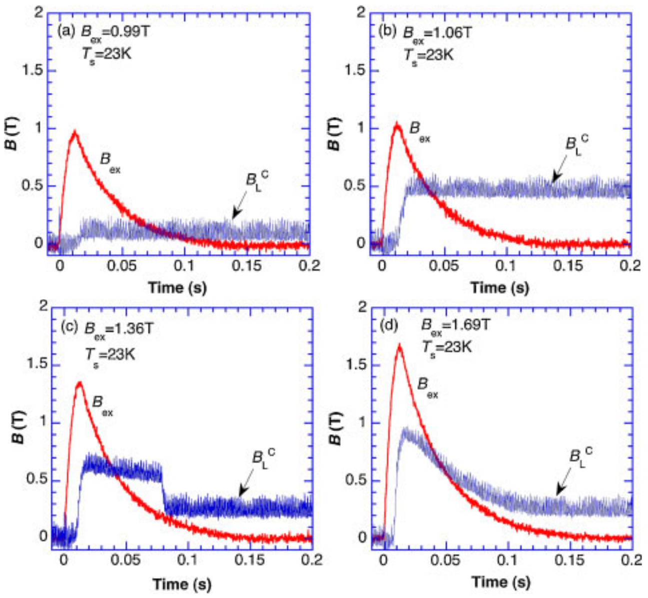

Fig. 3. (Color online) Time dependence of the applied field $B_{ex}(t)$ and the local field $B_L{}^C(t)$ at the center of the bulk surface at $T_s = 23$ K for (a) $B_{ex} = 0.99$ T, (b) 1.06 T, (c) 1.36 T, and (d) 1.69 T.

All the $B_L{}^C(t)$ were noisy because of insufficient electrical shielding. For each condition, $B_L{}^C(t)$ starts to increase for $t \geq 0.01$ s with a time delay, takes a maximum at 0.02 s, and then decreases to a final value due to the flux flow. It should be noted that, for $B_{ex} = 1.36$ T as shown in Fig. 3(c), the abrupt $B_L{}^C(t)$ drop was observed at $t = 0.08$ s because of the flux jump.

Figure 4 presents the trapped field profiles B_z (1 mm) on the surface of the MgB_2 bulk at $T_s = 23$ K for various applied fields B_{ex}. For a lower applied field of $B_{ex} = 0.99$ T shown in Fig. 4(a), a small amount of magnetic flux was mainly trapped at the coordinates of $(-10, -10)$. For $B_{ex} = 1.06$ T shown in Fig. 4(b), where the trapped field shows a maximum at $T_s = 23$ K as shown in Fig. 2, the magnetic flux was trapped mainly on the oblique line (region A) together with several spots around the periphery. For $B_{ex} = 1.36$ T shown in Fig. 4(c), the magnetic flux was trapped mainly around the bulk periphery, and for $B_{ex} = 1.69$ T shown in

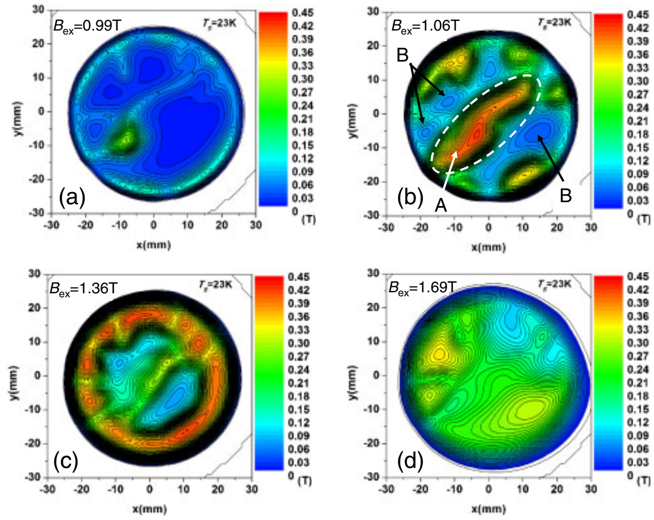

Fig. 4. (Color online) Trapped field profiles B_z (1 mm) on the surface of the MgB_2 bulk at $T_s = 23$ K for various applied fields B_{ex}.

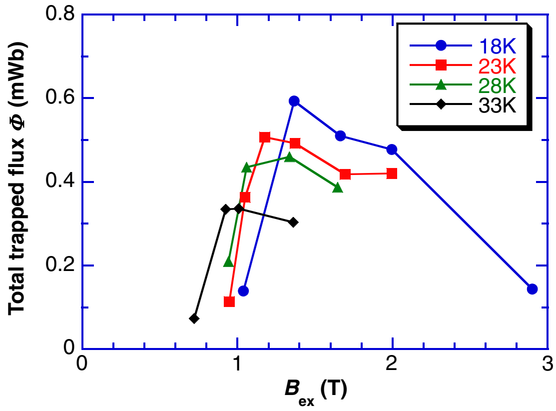

Fig. 5. (Color online) Total trapped flux Φ just above 1 mm from the bulk surface for each starting temperature T_s, as a function of applied pulsed field B_{ex}.

Fig. 4(d), the magnetic flux escaped and was re-distributed owing to the temperature rise. These results indicate that region A has a lower J_c and region B, as shown in Fig. 4(b), has a relatively higher J_c. Because, from the analogy in the REBaCuO bulks during PFM, the magnetic flux was trapped mainly around the growth sector region (GSR) with a lower J_c for the lower magnetic pulse application, then the trapped flux region was inclined at 45° to the growth sector boundary (GSB) with a higher J_c for the higher magnetic field. If the J_c is ideally homogeneous in the bulk, the trapped field profile should show a concave profile for a lower B_{ex} and a convex profile for a higher B_{ex}, according to the Bean model. These results shown in Fig. 4 suggest that the present MgB_2 bulk fabricated by the Mg-RLI method was inhomogeneous for the J_c distribution, which may result from the inhomogeneous infiltration of the Mg liquid.

Figure 5 shows the total trapped flux Φ on the surface of the MgB_2 bulk at $T_s = 23$ K for various applied fields B_{ex}, which was calculated by integrating the magnetic flux density B_z (1 mm) over the region where it was positive. All the Φ–B_{ex} curves take a maximum and then decrease with increasing B_{ex}. The maximum Φ value increases and the B_{ex}

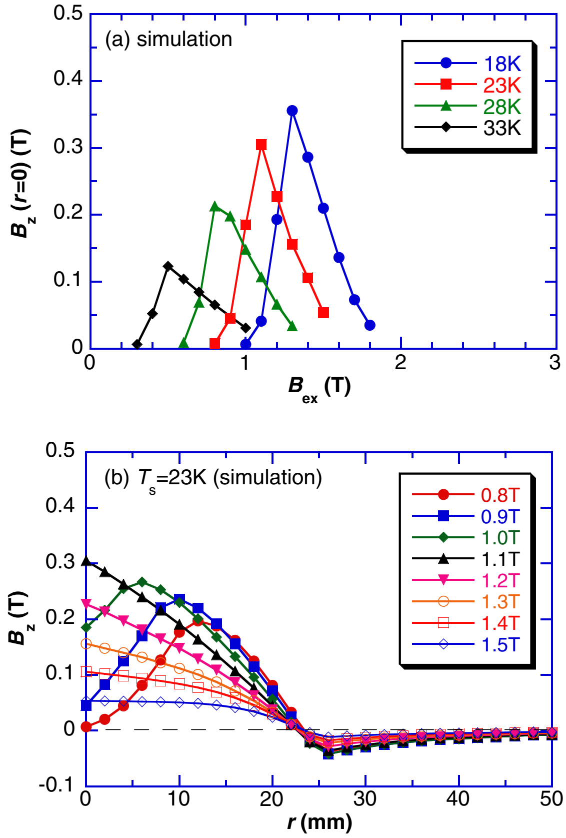

Fig. 6. (Color online) Results of the simulation of the (a) trapped field B_z at the center of the bulk surface as a function of the applied field B_{ex} for various T_s and (b) cross-sections of the trapped field $B_z(r)$ at $T_s = 23$ K for various B_{ex}.

value, at which Φ takes a maximum, shifts to a higher value with decreasing T_s.

5. Results of Numerical Simulation and Discussion

We present the results of the numerical simulation for a MgB_2 bulk during PFM. Figure 6(a) depicts the results of the simulation of the trapped field B_z ($r = 0$) at the center of the bulk surface as a function of the applied field B_{ex} for various starting temperatures T_s. In all the cases, B_z ($r = 0$) starts to increase concomitantly with increasing B_{ex}, becomes maximum, and then decreases with a further increase in B_{ex}. The critical applied field B_{ex}^0, at which the magnetic flux starts to trap at the bulk center, decreases concomitantly with increasing T_s. The results of the simulation reproduce qualitatively the experimental ones shown in Fig. 2.

Figure 6(b) presents cross sections of the trapped field profile $B_z(r)$ at $T_s = 23$ K for various B_{ex}. The positions of $r = 0$ and 25 mm are, respectively, the center and the edge of the bulk surface. The $B_z(r)$ profile changes from concave for a lower B_{ex} to convex for a higher B_{ex} and then the B_z ($r = 0$) value decreases with a further increase in B_{ex}. These behaviours are apparent for each T_s, but are not always strictly consistent with the experimental ones, as shown in Fig. 4, where region A was estimated to have a low J_c. In this study, the numerical simulation was performed under the ideal condition, in which the J_c value was homogeneous in the bulk. However, the results of the numerical simulation roughly reproduced the experimental ones.

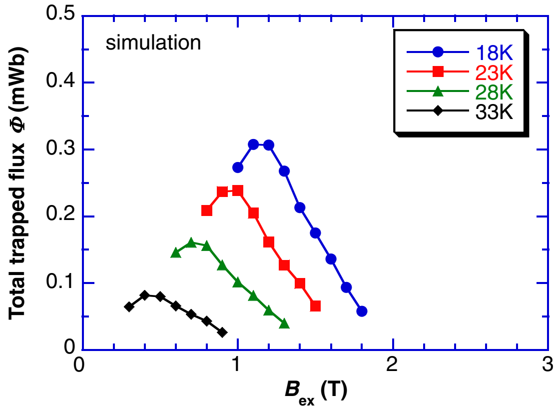

Fig. 7. (Color online) Results of the simulation of applied field dependence of the total magnetic flux Φ for various T_s.

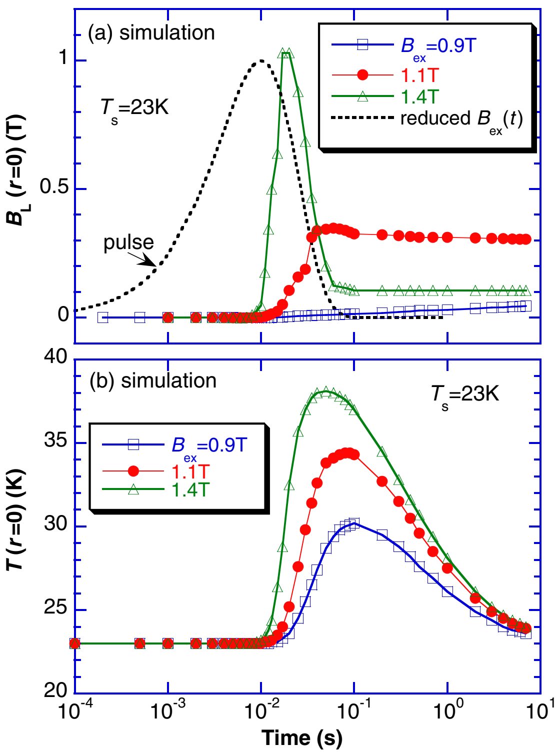

Fig. 8. (Color online) Results of the simulation of time dependence of (a) the local field $B_L^C(t)$ and (b) the temperature $T(t)$ at the center of the bulk surface at 23 K for a typical applied field B_{ex}.

Figure 7 shows the results of the simulation of the applied field dependence of the total magnetic flux Φ for various T_s. All the Φ–B_{ex} curves take a maximum and then decrease with increasing B_{ex}. The maximum Φ value increases and the B_{ex}^P value, at which Φ takes a maximum, shifts to a higher value with decreasing T_s. The B_{ex}^P value for each T_s is slightly lower than B_{ex}, at which B_T^C takes a maximum. These behaviours are qualitatively consistent with the experimental ones, as shown in Fig. 5.

Figures 8(a) and 8(b) show, respectively, the time dependences of the local fields $B_L^C(t)$ and the temperatures $T(t)$ at the center of the bulk surface at $T_s = 23$ K for a typical applied field B_{ex}. The time dependence of the reduced magnetic pulse $B_{ex}(t)$ is also shown. In Fig. 8(a), the local field

$B_L{}^C(t)$ starts to increase rapidly with a time lag for $B_{ex} = 1.1$ and 1.4 T and then decreases. In Fig. 8(b), the temperature $T(t)$ at the bulk center starts to rise rapidly and then decreases. The temperature starts to rise at $t = 0.01$ s, at which $B_{ex}(t)$ takes a maximum. $T(t)$ takes a maximum at $t =$ 0.07–0.1 s, which becomes shorter with increasing B_{ex}. For $B_{ex} = 1.4$ T, a steep decrease in $B_L{}^C(t)$ results from the approach of the temperature to $T_c = 39$ K. In this case, the temperature at the bulk periphery exceeded T_c and most of the trapped flux escaped from the bulk. The results of the simulation of the MgB_2 bulk were in clear contrast with those for REBaCuO bulks;[17] the applied field dependence of the trapped field was broad and the temperature $T(t)$ takes a maximum at 7 s. The differences come from the large thermal conductivity, small specific heat, and narrow temperature margin against the transition temperature T_c in the MgB_2 bulk. It is possible to add the secondary phases in the bulk to reduce the thermal conductivity and to enhance the specific heat. As a result, the temperature rise decreases during PFM and the trapped field will increase. The use of numerical simulation can optimize the operating parameters for PFM to enhance the trapped field.[17] MgB_2 bulk magnets are expected to be applicable in magnetically levitated trains and so on using liquid H_2 or cryocooler cooling.

6. Conclusions

Pulsed field magnetization (PFM) was performed for the first time for a large MgB_2 bulk of 50 mm diameter fabricated by a reactive liquid Mg infiltration (Mg-RLI) method, and the trapped field properties were measured. Important results of experiment and simulation and conclusions obtained in this study are summarized as follows.

(1) The maximum trapped field of $B_z = 0.47$ T was realized at the center of the bulk surface and the total trapped flux $\Phi = 0.5$ mWb was achieved at $T_s = 23$ K. Both values decreased with increasing temperature T_s.

(2) The experimental results can be roughly reproduced by numerical simulation using electromagnetic and thermal fields, although inhomogeneous J_c distribution exists in the present MgB_2 bulk fabricated by the Mg-RLI method from the trapped field profiles by PFM.

(3) The flux dynamics and the heat generation/propagation of the MgB_2 bulk during PFM were in clear contrast with those for REBaCuO bulks because of the large thermal conductivity, small specific heat, and narrow temperature margin against the transition temperature T_c in the MgB_2 bulk. In the future, using liquid H_2, high-strength MgB_2 bulk magnets are expected for practical applications.

Acknowledgment

This work is supported in part by a Grant-in-Aid for Scientific Research (No. 23560002) from the Ministry of Education, Culture, Sports, Science and Technology, Japan.

1) Y. Yanagi, T. Matsuda, H. Hazama, K. Yokouchi, M. Yoshikawa, Y. Itoh, T. Oka, H. Ikuta, and U. Mizutani: Physica C **426–431** (2005) 764.
2) F. Mishima, S. Takeda, Y. Izumi, and S. Nishijima: IEEE Trans. Appl. Supercond. **17** (2007) 2303.
3) H. Hayashi, K. Tsutsumi, N. Saho, N. Nishijima, and K. Asano: Physica C **392–396** (2003) 745.
4) D. Litzkendorf, T. Habisreuther, J. Bierlich, O. Surzhenko, M. Zeisberger, S. Kracunovska, and W. Gawalek: Supercond. Sci. Technol. **18** (2005) S206.
5) M. Kambara, N. Hari Babu, E. S. Sadki, J. R. Cooper, H. Minami, D. A. Cardwell, A. M. Campbell, and I. H. Inoue: Supercond. Sci. Technol. **14** (2001) L5.
6) R. V. Viznichenko, A. A. Kordyuk, G. Fuchs, K. Nenkov, K.-H. Muller, T. A. Prikhna, and W. Gawalek: Appl. Phys. Lett. **83** (2003) 4360.
7) A. Yamamoto, H. Yumoto, J. Shimoyama, K. Kishio, A. Ishihara, and M. Tomita: Abstr. 23rd Int. Symp. Superconductivity, 2010, p. 219.
8) G. Giunchi: Int. J. Mod. Phys. B **17** (2003) 453.
9) E. Perini, G. Giunchi, L. Saglietti, A. Albisetti, A. Matrone, and V. Cavaliere: IEEE Trans. Appl. Supercond. **21** (2011) 2690.
10) Y. Yanagi, Y. Itoh, M. Yoshikawa, T. Oka, T. Hosokawa, H. Ishihara, H. Ikuta, and U. Mizutani: *Advances in Superconductivity XII* (Springer, Tokyo, 2000) p. 470.
11) M. Sander, U. Sutter, R. Koch, and M. Klaser: Supercond. Sci. Technol. **13** (2000) 841.
12) H. Fujishiro, T. Oka, K. Yokoyama, M. Kaneyama, and K. Noto: IEEE Trans. Appl. Supercond. **14** (2004) 1054.
13) H. Fujishiro, T. Hiyama, T. Miura, T. Naito, S. Nariki, N. Sakai, and I. Hirabayashi: IEEE Trans. Appl. Supercond. **19** (2009) 3545.
14) H. Fujishiro, T. Hiyama, T. Tateiwa, Y. Yanagi, and T. Oka: Physica C **463–465** (2007) 394.
15) H. Fujishiro, M. Kaneyama, T. Tateiwa, and T. Oka: Jpn. J. Appl. Phys. **44** (2005) L1221.
16) H. Fujishiro, T. Tateiwa, A. Fujiwara, T. Oka, and H. Hayashi: Physica C **445–448** (2006) 334.
17) H. Fujishiro and T. Naito: Supercond. Sci. Technol. **23** (2010) 105021.
18) H. Fujishiro, T. Naito, and M. Oyama: Supercond. Sci. Technol. **24** (2011) 075015.
19) H. Fujishiro, T. Naito, and D. Furuta: IEEE Trans. Appl. Supercond. **21** (2011) 2723.
20) T. Cavallin, E. A. Young, C. Beduz, Y. Yang, and G. Giunchi: IEEE Trans. Appl. Supercond. **17** (2007) 2770.
21) Y. Komi, M. Sekino, and H. Ohsaki: Physica C **469** (2009) 1262.
22) I. Iwayama, S. Ueda, A. Yamamoto, Y. Katsura, J. Shimoyama, and K. Kishio: Physica C **460–462** (2007) 581.
23) G. Giunchi, S. Ceresara, G. Ripamonti, S. Chiarelli, and M. Spadoni: IEEE Trans. Appl. Supercond. **13** (2003) 3060.
24) Ch. Wälti, E. Felder, C. Degen, G. Wigger, R. Monnier, B. Delley, and H. R. Ott: Phys. Rev. B **64** (2001) 172515.